The Astrophysical Journal, 939:14 (14pp), 2022 November 1 https://doi.org/10.3847/1538-4357/ac930a

The Evolution of the Optical Spectrum of V455 Andromedae throughout the 2007 Superoutburst

Gagik Tovmassian[1], Boris T. Gänsicke[2], Juan Echevarria[3], Sergey Zharikov[1], and Abdiel Ramirez[1]
[1] Instituto de Astronomía, Universidad Nacional Autónoma de México, Aptdo Postal 106, Ensenada, Baja California, C.P. 22800, Mexico; gag@astro.unam.mx
[2] University of Warwick, Department of Physics, Gibbet Hill Road, Coventry, CV4 7AL, UK
[3] Instituto de Astronomía, Universidad Nacional Autónoma de México, Aptdo Postal 70-264, Ciudad Universitaria, CDMX, C.P. 04510, México
Received 2022 June 23; revised 2022 September 17; accepted 2022 September 19; published 2022 October 27

Abstract

V455 And is a dwarf nova with a short orbital period, close to the orbital period minimum. The object underwent its first detected outburst in 2007, brightening from around $V = 16.5$ all the way to magnitude 8. Outbursts of such amplitude occur exclusively in dwarf novae with short periods (typically $P_{\rm orb} \lesssim 90$ minutes) and are called superoutbursts. The recurrence time of superoutbursts is long (decades), hence only very few have been studied in detail. We succeeded in observing the entire superoutburst of V455 And spectroscopically from the rise to the decline with unprecedented detail. While the light curve of the object throughout the outburst does not seem to differ much from other dwarf novae, its spectroscopic behavior is strikingly different during the transition stage from the absorption-dominated lines to the strong emission one during the rise. We interpret the emergence of the strong emission lines with little radial velocity variations during the superoutburst as evidence of wind from the evaporating disk in this high-inclination system. The evolution of the line profiles from wide to narrow peak separation during the rise, and back at the decline, matches models showing that the peak separation is a function of optical depth in the lines.

Unified Astronomy Thesaurus concepts: Cataclysmic variable stars (203)

1. Introduction

Cataclysmic variables (CVs) are close binary systems comprised of a white dwarf (WD) and a low-mass main-sequence star or a brown dwarf. The latter fills its Roche lobe and loses matter via the inner Lagrangian point to the more massive primary component of the binary system (Warner 1995). In the absence of a magnetic field on the WD, this material forms an accretion disk around the WD. Accretion disks are sources of noticeable variability, spanning a range in amplitudes and timescales, from high-frequency quasi-periodic oscillations in the inner disk, to tidal distortions of the entire disk, to outbursts and superoutbursts. If the WD is weakly magnetic (a few 100 kG to a few MG), the field disrupts the inner disk, from where it then channels the material onto the magnetic poles of the WD (Hellier 2002). This multicomponent accretion structure, combined with additional variability on the binary and stellar rotation periods, produces a very complex observational behavior.

The subject of this paper, V455 And, has been a champion in terms of the number of observed periodicities and variability (Araujo-Betancor et al. 2005; Bloemen et al. 2013), including the first recorded superoutburst (Matsui et al. 2009). This behavior immediately enlisted V455 And as a WZ Sge–type CV. WZ Sge stars have supercycles (time between superoutbursts) that last decades, while normal outbursts are few or absent altogether. WZ Sge itself has had a superoutburst at intervals of about 30 yr, and it has never been seen to undergo a normal outburst. Other WZSge–type stars, including GW Lib, AL Com, and EG Cnc, have been thought to have superoutburst intervals of approximately 20 yr. However, Al Com underwent an unusual outburst with a recurrence time of only 1.5 yr, the shortest interval of superoutbursts among WZ Sge–type dwarf novae (Kimura et al. 2016). Another exception is EZ Lyn exhibiting superoutbursts 4 yr apart (Isogai et al. 2015). Kato (2015) presents a list of almost 100 WZ Sge objects and the properties of their light curves. Only very few of them have been observed spectroscopically during the superoutburst.

It is widely accepted that dwarf nova (DN) outbursts are caused by a thermal instability in the accretion disk when the central temperature is of the order of the ionization temperature of hydrogen, and the opacities are strongly dependent on temperature. The idea of the disk instability model (DIM) was formulated back at the beginning of the 1980s by various authors, including Meyer & Meyer-Hofmeister (1981), Smak (1982), and Mineshige & Osaki (1983), among others (see the latest review on DIM by Hameury 2019). Osaki (1995) suggested the combination of DIM with the tidal instability of the disk for a short-period DN to explain a succession of outbursts and superoutbursts in WZ Sge–type CVs and, as an extreme case, of SU UMa objects. While the influence of tidal instability on the occurrence and peculiarities of the outburst course is debatable (Hameury 2019), tidal instability constitutes itself in various forms of superhumps observed during superoutbursts (Matsui et al. 2009). Another interesting feature of V455 And and its archetype WZ Sge is that they have a truncated accretion disk due to the magnetic field of their WD and both experience superoutbursts (Kuulkers et al. 2011; Hameury & Lasota 2017).

Regardless, it is understood that CVs near the orbital period minimum at around 80 minutes also reach the lowest accretion rates, extreme mass ratio, and, consequently, low viscosity of the accretion disks (as low as $\alpha_{\rm cold} \approx 0.001$ in quiescence). When the temperature and surface density reaches the point of instability, the outburst commences by transitioning the disk into an optically thick state. It is constituted by gradually

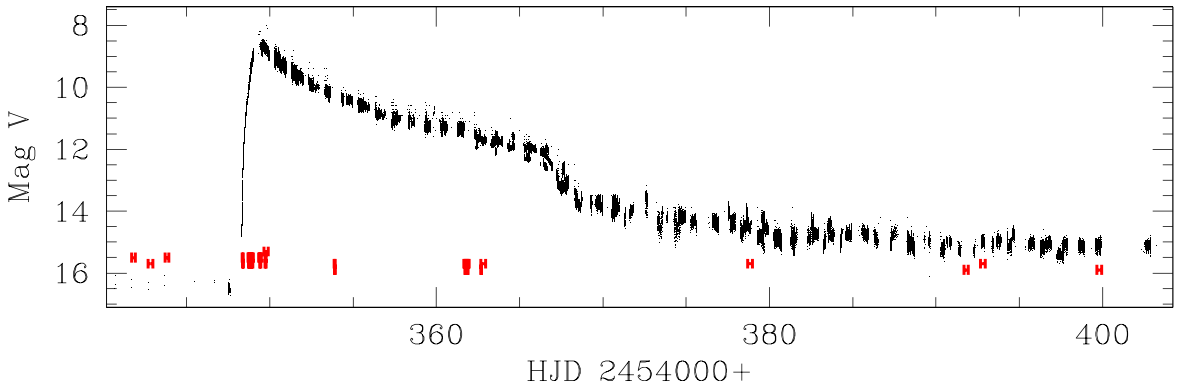

Figure 1. The light curve of V455 And during the 2007 superoutburst. The black points are publicly available data from AAVSO. The red bars at the bottom show the moments of spectroscopic observations before and during the superoutburst.

converting the emission lines formed in the disk into absorption features as the instability wave propagates throughout the disk, ionizing the gas. When the disk entirely turns optically thick, shallow and wide absorption features dominate, or sometimes it is a mix of absorption and emission, resulting in an almost featureless blue continuum very much like spectra of novalikes with permanently hot and dense disks. There are only a few examples of spectra of WZ Sge type during superoutbursts (Szkody et al. 1996; Nogami & Iijima 2004; Liu et al. 1997; Steeghs et al. 2001; Kuulkers et al. 2002; van Spaandonk et al. 2010).

We obtained an unprecedented dense spectroscopic coverage of the 2007 superoutburst by V455 And. The superoutburst was caught early in the rise, which is rare. Here we report the results of spectroscopic monitoring of the superoutburst from the first day, when it was only a magnitude above its quiescent level, through the peak and decline during 40 days.

2. System Properties of V455 And

V455 And is an 81 minute-period DN located at 75.82 ± 0.28 pc (Gaia Collaboration et al. 2018). Araujo-Betancor et al. (2005) and Gänsicke (2007) suggested a primary with $M_{\rm wd} = 0.6\ M_{\odot}$ and an L2 secondary, based on fitting the spectral energy distribution. Their estimate adopted a distance $d \approx 90 \pm 15$ pc, derived from modeling the emission of the WD. The orbital period is close to the minimum for CVs with hydrogen-rich WDs. Hence, V455 And shares the basic characteristics of WZ Sge–type objects, all of which cluster around ≈80 minutes.

We paid particular attention to the precision of the orbital period determination. The duration of the superoutburst, as well as our corresponding observations, spans 60 days. The object, with an ≈80 minute period, completes more than 1000 cycles during our observations, and we must ensure that the phases of individual spectra we use to produce Doppler tomograms remain correct during the entire interval of our spectroscopy. The ephemeris derived by Araujo-Betancor et al. (2005) was recently refined using the eclipse timing from the TESS observations and the wealth of preceding data. The light-curve models (G. Tovmassian et al. 2022, in preparation) demonstrate that the true stellar conjunction is shifted by $\Delta\phi = -0.055$ with respect to the grazing eclipses reported by Araujo-Betancor et al. (2005). The newly deduced precise values derived from 122,563 orbital cycles are $T_0({\rm HJD}) = 2458714.10055$ and $P_{\rm orb} = 0.05630918711$ days.

Tovmassian et al. (2022, in preparation) also used a precise Gaia distance to reevaluate the binary parameters from the light-curve and SED modeling, which now stand at $M_{\rm wd} = 0.77 - 0.83\ M_{\odot}$, a mass ratio $q = 0.07 - 0.064$, and an inclination angle $i = 70.^{\circ}8$.

An outstanding feature of V455 And is the presence of a second period, unrelated to the orbital period, associated with the variability of the radial velocity of emission lines, which we call the long spectroscopic period (LSP). This additional variability is detected at around 3.5 hr (Araujo-Betancor et al. 2005). This period is stable but drifts on timescales of days. A double spectroscopic period has been so far detected only in one other CV: FS Aur (Tovmassian et al. 2007). In order to understand the characteristics of the LSP and its physical origin, we have been conducting regular spectroscopy of V455 And since 2004. The results of that study will be reported by G. Tovmassian et al. 2022, in preparation.

The course of the outburst is shown in Figure 1. The amplitude and the duration are typical of a WZ Sge–type superoutburst. During the superoutburst, additional photometric periodic variability was detected in the form of superhumps in the object's light curve. Superhumps of different types are characteristic of SU UMa and WZ Sge light curves. A comprehensive study of these tidal accretion disk variabilities has been published by Matsui et al. (2009).

The entire light curve can be divided into a few distinct phases: rise to outburst, peak, rapid decline converting into slower fading, rapid drop in brightness, followed by another slow fading. These phases are commonly observed in the superoutbursts of WZ Sge–type systems (Bailey 1979). However, unlike many other WZ Sge stars observed in superoutburst, V455 And did not show echo outbursts during fading. Details on the photometric behavior of V455 And and the morphology of its light curve can be found in Matsui et al. (2009). We obtained spectra practically during all of the outburst phases, which we describe in the following section, starting from the pre-outburst spectra obtained only 5 days before the superoutburst.

3. Observations and Data Presentation

The light curve and the V magnitudes have been obtained through the AAVSO (Kafka 2021) and our own observations at the 1.2 m Kryoneri telescope in Greece. The photometric observations from Kryoneri provided the outburst alert and triggered follow-up observations. The photometric data were reduced with a pipeline that employs bias subtraction, dark

Table 1
Spectroscopic Observations of V455 And (The Outburst)

Date 2007	JD 2450000+	Start Time UT	End Time UT	Instrument	Range (Å)	Exposure Time (s)	No. of Spectra
Aug 10	4322	07:08	12:20	OAN/SPM 1.5 m, B&Ch	3975–6075	420	41
Aug 11	4323	06:07	12:11	OAN/SPM 1.5 m, B&Ch	3976–6073	420	49
Aug 12	4324	06:01	12:09	OAN/SPM 1.5 m, B&Ch	3976–6073	420	50
Aug 29	4341	06:42	09:27	OAN/SPM 2.1 m, B&Ch	3740–5835	420	20
Aug 30	4342	04:55	11:29	OAN/SPM 2.1 m, B&Ch	3740–5835	420	52
Aug 31	4343	05:01	09:42	OAN/SPM 2.1 m, B&Ch	3740–5835	420	29
Sep 4	4348	20:21	06:36	WHT 4.2 m, ISIS R600B	3965–5700	180	161
Sep 5	4348	06:16	12:20	OAN/SPM 2.1 m, B&Ch	4000–5595	50–120	181
Sep 5	4349	20:12	06:35	WHT 4.2 m, ISIS R600B	3965–5700	60	860
				WHT 4.2 m, ISIS R600R	5770–7420		860
Sep 6	4349	04:42	11:15	OAN/SPM 2.1 m, Echelle	3800–6850	240	49
Sep 10	4353	08:32	10:22	OAN/SPM 2.1 m, B&Ch	3765–5760	120	42
Sep 18	4361	03:54	11:02	OAN/SPM 2.1 m, B&Ch	3765–5760	120	91
Sep 19	4362	03:45	10:58	OAN/SPM 2.1 m, B&Ch	3765–5760	120	97
Oct 5	4378	04:36	11:12	OAN/SPM 2.1 m, B&Ch	3960–5554	240	80
Oct 18	4391	02:36	10:17	OAN/SPM 2.1 m, B&Ch	4000–5594	360	66
Oct 19	4392	02:22	10:21	OAN/SPM 2.1 m, B&Ch	4000–5594	360	75
Oct 25	4398	03:16	11:00	OAN/SPM 2.1 m, B&Ch	4000–5594	360	70
Oct 26	4399	02:23	09:43	OAN/SPM 2.1 m, B&Ch	4000–5594	360	70

current subtraction, and flat-fielding in the standard fashion within MIDAS and uses SEXTRACTOR (Bertin & Arnouts 1996) to perform aperture photometry. Five days before the superoutburst and throughout the entire campaign we observed V455 And from the Observatorio Astronómico Nacional de San Pedro Mártir (OAN SPM), México. Phase-resolved spectra of V455 And were obtained with the 2.1 m telescope and the intermediate dispersion spectrograph by Boller & Chivens, using a 400 l mm^{-1} grating in the second order and a BG39 filter, to deliver a wavelength coverage of about 1600 Å centered around 4600 Å thus including several Balmer lines as well as neutral and ionized helium lines. The SITe3 1 kV CCD was used to acquire the data with 1.55 Å per pixel resolution.

V455 And was observed continuously, covering several orbital cycles, each time we had a night allocated at the telescope. A CuHeNeAr arc lamp was taken once every dozen object exposures, and one spectroscopic standard was observed per night. The exposures varied depending on the object's brightness but were always much shorter than the orbital period. Such modus operandi was maintained during the entire observing cycle covering the superoutburst.

On September 6, around the outburst's peak, observations were carried out at SPM using the higher-resolution Echelle spectrograph($R \sim 12{,}000$). The SITe3 CCD 1024×1024 pixels were used to obtain 49 spectra in the region 3800–6850 Å, using the echellette grating of 300 l mm^{-1}. The exposure time for the individual spectra was 240 s. The log of observations with details of exposure times, spectral range, and resolutions is presented in Table 1.

The early stage of rising during the superoutburst was also observed using the Intermediate Dispersion Spectrograph and Imaging System (ISIS) on the 4.2 m William Herschel Telescope (WHT) on La Palma covering $\sim 8 + 8$ orbital periods on September 4 and 5. The wavelength range 3965–5835 Å was used, sampled at a 1.8 Å resolution (FWHM; 1.″0 slit) with a 2048×4200 pixel EEV12 CCD. Arc lamp spectra were regularly taken in order to achieve an accurate wavelength calibration. No spectroscopic standard was observed, and hence, the WHT spectra were not flux-calibrated. Thereafter, all of the following spectroscopy was obtained at OAN SPM.

We obtained a total of ≈2000 spectra throughout the superoutburst. In order to present them in a meaningful and illustrative manner, we have made use of Doppler tomography (Marsh & Horne 1988) as an instrument to demonstrate changes taking place in the spectroscopic behavior of V455 And over two months, starting with the pre-outburst, the following maximum, decline, and almost down to the quiescent level. This study uses the reconstruction method based on the maximum entropy principle (Spruit 1998). In addition to the usual contour of the secondary star, the center of mass, the location of the stellar components, and the arc lines indicating the ballistic and Keplerian trajectories of the accretion stream, the circle showing the disk truncation radius (external) of the accretion disk according to Paczynski (1977) and Neustroev & Zharikov (2020) is also drawn in all maps.

4. Spectral Evolution of V455 and during the Superoutburst

4.1. Pre-outburst Spectra

We had the luck to obtain spectrophotometric observations of V455 And five days before the start of the superoutburst. This was merely by chance as we were observing the object and had no foreknowledge that a superoutburst was about to start. We also had photometric observations 18 hr prior to discovering that the object was indeed going into superoutburst. The labels presented in the first column of Table 2 define certain stages of the rise. We use these labels in the following text for clarity. We have assigned the label zero to the quiescence observations of V455 And both spectral and photometric in Table 2, although they do not coincide exactly in time.

At label zero, the object displayed similar behavior to previous observations, i.e., broad double-peaked Balmer

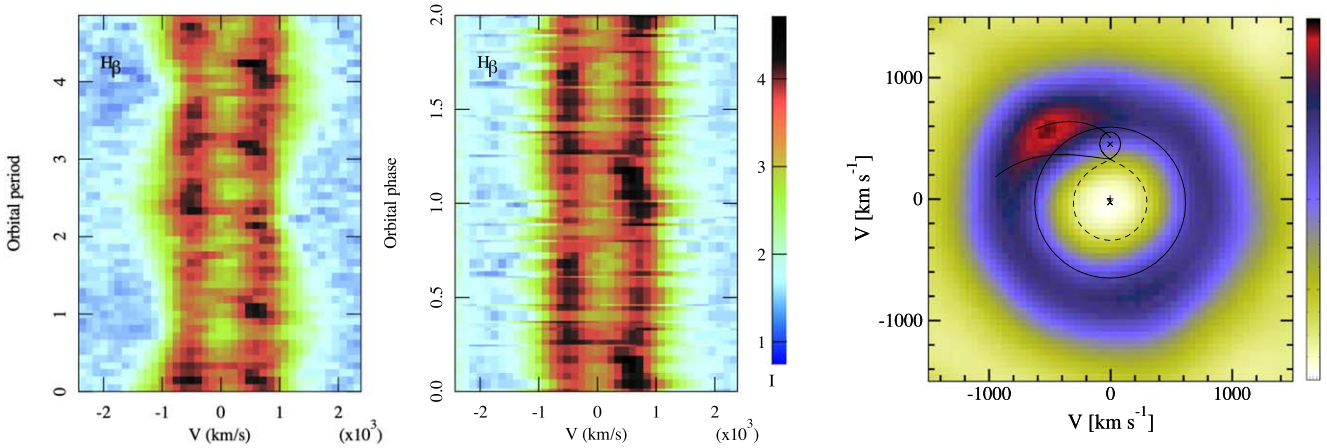

Figure 2. Spectroscopy covering Hβ was obtained on August 30, i.e., 5 days before the start of the superoutburst. On the left, the trailed spectrum is shown without period folding (with the time axes in units of orbital periods), while in the middle panel it is folded with the orbital period. The right panel shows the Doppler tomogram corresponding to the period-folded trailed spectrum. The Roche lobe of the donor star is traced by a solid line, that of the WD by a dashed line, and the two crosses mark the center of mass and the WD. The ballistic and Keplerian trajectories of the accretion stream are indicated by arc lines. The solid circle shows the (external) truncation radius of the accretion disk.

Table 2
Essential Moments of the Rise to the Superoutburst of V455 And

Label	HJD 2454000+	Time since the First Spectrum (hr)	Brightness *V* Magnitude	Comments
0	343.833	−108.368	(16.4)	quiescence spectral
0	347.576	−18.536	16.49 ± 0.05	quiescence photometric
1	348.3483	0.0	13.895 ± 0.005	the 1st spectrum
2	348.3698	0.5164	13.113 ± 0.004	emission to absorption
3	348.4278	1.907	12.141 ± 0.006	
4	348.5840	5.655	10.924 ± 0.007	
5	348.7135	8.765	10.19 ± 0.005	emission+He II
6	349.0182	16.076	8.97	
7	349.4806	27.175	8.60	maximum

Note. The labels presented in the first column define certain stages of the rise. Label zero marks the quiescence. The second column presents the moment of the observation, the third column shows the difference in time of each stage with respect to the first outburst spectrum, the fourth column shows the brightness of the object at that moment, and the fifth column gives details of each stage.

emission lines with an intense S-wave component inside the line (Araujo-Betancor et al. 2005; Bloemen et al. 2013). The S-wave phasing suggests that this component arises from the bright spot formed as a consequence of the collision of the infalling mass-transfer stream with the accretion disk. The S-wave radial velocities (RV) varied according to the well-established orbital period (Araujo-Betancor et al. 2005; G. Tovmassian et al. 2022, in preparation). Meanwhile, the RV of the wings of lines swings with a much longer, distinct period. Trailed spectra and the corresponding Doppler tomogram are depicted in Figure 2. Since the object has two spectroscopic periods, we composed two trailed spectrograms of the Hβ line to illustrate both signals.

In the first case, we stacked all spectra in time (left panel of Figure 2). The LSP is clearly visible in the left panel as a wave in the wings of the line. Two cycles of the ∼240 minute LSPs were covered within the 6.6 hr observations obtained on 2007 August 30. The orbital period is visible in this trailed spectrum as an S wave inside the double-peaked line.

In the second case, the trailed spectrogram was produced by folding the spectra according to their orbital phases (middle panel of Figure 2) computed with the new ephemeris of G. Tovmassian et al. 2022, in preparation, where phase zero corresponds to inferior conjunction of the donor. The hot spot produces one S wave per orbit and the accretion disk appears as two vertical strips. The Doppler map created from the spectra folded on the orbital period clearly shows the presence of an accretion disk and a hot spot (right panel of Figure 2). We conclude that four days before the outburst, the binary system appeared similar to previous years with no indication of the upcoming cataclysm.

4.2. Early Rise to Outburst

On 2007 September 4 (HJD 2454348, hereafter HJD 348), when V455 And was found slightly brighter than 15th mag (Maehara et al. 2009), the team at WHT started monitoring what turned out to be a superoutburst. The times of spectroscopic observations are marked by red bars at the bottom of Figure 1. Many of these observations covered the system's orbital period (81.09 minutes =0.05631 days), and we will analyze each orbital cycle separately, given the rapid change and the unprecedented spectroscopic coverage we obtained.

4.3. Fast Rise

The rise of a DN to outburst is a very fast event and, therefore, difficult to catch photometrically and spectroscopically. Fortunately, we caught it in the earliest possible stages and were able to follow it almost without interruption in time. This paper focuses on spectroscopy; the photometric analysis will be published elsewhere. The first spectrum at this stage was obtained on HJD 2454348.3483 (labeled 1 in Table 2 and in subsequent figures). We obtained over 160 spectra during this initial rise and display a selection from the first one to 27 hr later in the right panel of Figure 3. A portion of the light curve detailing the rise to the superoutburst is shown in the bottom-left panel of the same figure. The measurements of equivalent

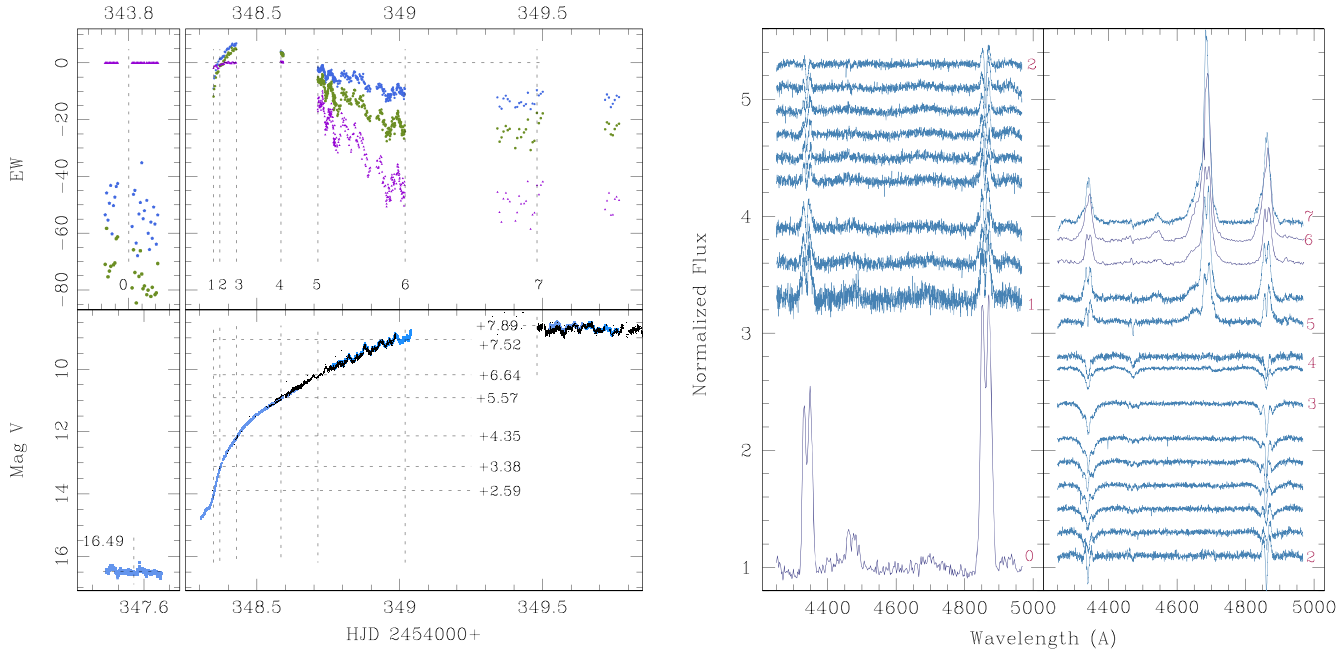

Figure 3. Photometric light curve and EW (left panels) and a sequence of spectra during the first 10 hr of monitoring (right panel). The light curve is a combination of our observations (blue) and the AAVSO (black). The EWs of three lines are shown color-coded as follows: He II—magenta; Hβ—green; Hγ—blue. The numbers from 0 to 7 and corresponding vertical dashed lines in the left panel mark certain moments of the light curve discussed in the text. The horizontal dashed lines indicate the brightness increase at the labels relative to the quiescence. The spectra from WHT in the right panel are normalized and offset vertically by suitable amounts to illustrate the evolution of the outburst. The spectra are stamped in accordance with the labels.

widths (EWs) are given in the upper-left panels. The vertical dashed lines indicate HJD times from column 2 of Table 2. The horizontal dashed lines in the bottom panels indicate the object's brightness at the marked moments. We show the quiescent values (label 0) in separate left panels to make the data sequence more illustrative.

The rise of V455 And can be characterized by fast and gradual phases. Our first outburst spectrum of the object was obtained before the beginning of the fast rise. The latter is marked by number 1 in the upper panel in Figure 3. There is a small but pronounced twig in the light curve before the fast rise. Maybe the initial rise was not very rapid, but we have insufficient data at this stage to explore our assertion. During the fast phase (labels 1–3), the brightness of the object rose at a 1.3 mag hr^{-1} rate, while later, the growth rate fell to a 0.3 mag hr^{-1}. Spectroscopically, the fast rise was manifested by a decreasing intensity of the emission lines and an absorption enhancement. Within 30 minutes of our first spectrum, the EWs of the absorption lines canceled the emission ones, until the EWs of the Balmer lines became zero. This happened at label 2. However, the widths of the emission and absorption components are different; hence the lines were still visible in the spectra as wide emissions with a deep absorption core in the center (see spectrum labeled 2 on the right side of Figure 3).

After this moment (label 2), the brightness kept increasing almost at the same pace (slightly slower); meanwhile, absorption features started to dominate the lines, and the EWs of the Balmer lines changes from negative to positive. At label 3, the Balmer and He I lines are predominantly wide absorption features, reaching the largest positive EW. Such a transition is common for DN outbursts and WZ Sge super-outbursts. According to the disk instability model (Hameury 2019), the propagation of a heating front rapidly ignites the whole disk. The physical interpretation is that the accretion disk switches from a cold and low-viscosity disk to a hot and high-viscosity disk. The disk keeps heating up because it has become entirely optically thick. At this moment, a change in pace occurs in the photometric light curve, a slowing down to the already mentioned 0.3 mag hr^{-1}. At this time, the He II line is still absent in the spectra.

We can visualize changes in the structure of the accretion disk during the fast rise using Doppler tomography. We constructed two tomograms of Hβ, each one encompassing an orbital period between labels 1 and 2. The time span was shorter than two full periods, hence they overlap. Nevertheless, the change is significant. In the first tomogram shown in Figure 4, the accretion disk was still prominent; the entire ring was visible, with the hot spot showing up at its regular place, where the infalling mass-transfer stream hits the disk, producing a shock. The disk was considerably weaker during the second orbit, and so was the hot spot. The He I λ4471 line had a weak emission component only during the first of these periods; it completely disappeared during the second one.

4.4. Gradual Rise

After a 3.85 hr gap in our observations, several spectra were taken around label 4. The lines become predominantly in absorption (note the behavior in the EWs of Hβ and Hγ). Otherwise, V455 And appears similar to before. Emission components from the disk have almost vanished. Super-outbursts are essentially similar to dwarf novae in outburst, which happens in disks of lower viscosity (Meyer & Meyer-Hofmeister 2015). The mechanism leading to the diminishing emission lines superimposed on broad absorption lines maintains the disk in a hot ionized state throughout the rise, plateau, and early decline. Observations of DN outbursts are not that rare, and they generally confirm the disk instability model, according to which the bulk of the hot steady-state disk

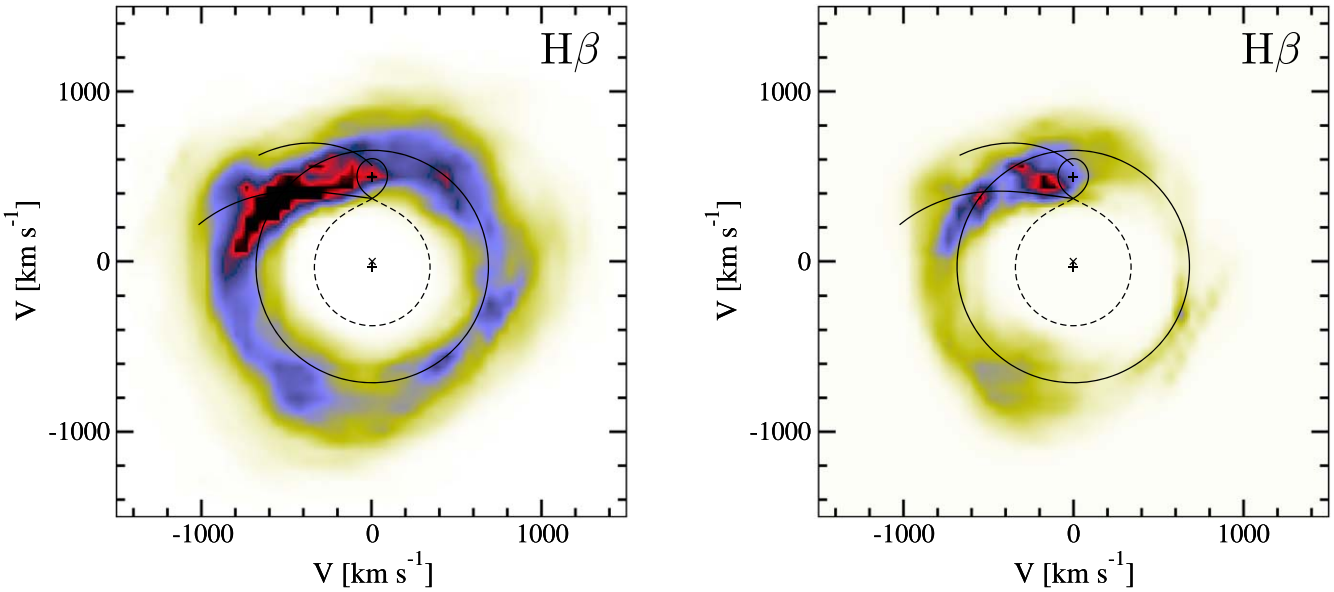

Figure 4. Doppler maps of V455 And for two overlapping orbital periods, 81 minutes each (all overlays have the same meaning as in Figure 2; see the text for details). The tomograms are produced from 24 spectra each. The image of the accretion disk is clearly visible in the form of a ring on the left-hand side, fading on the right-hand side. Extended emission in the top left of both tomograms corresponds to the hot spot.

produces absorption, rather than emission, lines (e.g., Morales-Rueda & Marsh 2002). Likewise, during the superoutburst of WZ Sge, the Balmer lines in the spectra turn into absorption and remain partially or fully in absorption during the maximum plateau and the early fading, even if He II λ4686 appears in emission (Echevarría et al. 2002; Nogami & Iijima 2004; Nogami et al. 2009).

Observations resumed after another $\simeq$3.1 hr gap, i.e., $\simeq$8.8 hr since the first spectrum was taken (label 5 in Table 2 and shown in Figure 3). At this time, significant changes in the spectra take place. First and foremost, the He II λ4686 line shows up strongly, with the usual company of the complex C III/N III blend around 4640 Å. Double-peak Balmer lines appear in emission at label 5, while He I lines remain in absorption. From labels 5 to 6, the brightness of the object rises steadily as well as the intensities of the emission lines. At the same time, early superhumps appear in the light curve (Maehara et al. 2009), which are reflected in the EWs of the lines. The EWs of lines grow in a zigzag, concurring with the variation of the underlying continuum. The early superhumps are thought to be the result of the emergence of spiral patterns caused by the 2:1 resonance due to an increased disk radius (Lin & Papaloizou 1979). One can assume that the line growth is unrelated to the continuum variability. In the course of 7 hr, the brightness rises by almost a magnitude, while the EW of the He II line increases from ≈ -15 to ≈ -45 Å.

The emergence of these strong emission lines (best demonstrated by a trailed spectrum in Figure 5), while the brightness is still on the rise (the interval between points 5 and 6), is remarkable. In particular we note the appearance of additional two He II lines at λ4200 and λ4541 as depicted in Figure 6. These recombination lines are usually formed for electron temperatures and densities appropriate for winds and are typically observed in hot stars with high mass loss. These two lines do not come alone; there are many coincidences with He II λ4686, λ5412 and the Balmer lines, as marked in Figure 6. Accretion disk-wind models predict the presence of these recombination lines in the optical spectrum (Matthews et al. 2015) but are rarely found in CVs except, e.g., V Sge, a CV with a massive secondary emitting strong stellar wind (see Echevarría et al. 1989 and references therein).

Figure 7 shows a series of Doppler maps of hydrogen and ionized helium during this transformation of the lines. The sequence of Doppler maps starts chronologically at the bottom of the figure, corresponding to the first observed orbital period on HJD 348.74 at label 5 and ends seven orbits later at label 7 (JD 349.74). The ring of emission in the Doppler maps usually denotes the disk (see the bottom rows); however, it has a smaller radius than during quiescence (Bloemen et al. 2013). The ring is uneven, somewhat reminiscent of the spiral structure discussed by Steeghs (2004). However, this ring velocity is too low, and its structure does not last more than two orbital periods. It starts to shrink rapidly, as seen in the sequence of images from the bottom up in Figure 7. After just a few orbits, it forms almost a circular spot with zero velocity. This phenomenon is observed in all Balmer lines as well as in the He II λ4686 line. That in itself contradicts both theoretical predictions (Cheng & Lin 1992) and the observed behavior of accretion disks (Martinez-Pais et al. 1996) during outbursts: The increased mass and angular momentum flow through the disk results in an increase in the disk radius. Thus, we argue that the velocity of the emitting gas seen in the Doppler maps of V455 And is smaller than a Keplerian disk velocity, and consequently, the gas that causes this emission is not located within the disk.

4.5. The Maximum

The system reached maximum brightness around label 7, i.e., about 27 hr after our first spectrum was taken. At this stage, the emission lines become wider and practically single peaked. It is at this point, around the maximum of the outburst, that the high-resolution echelle spectra, which reveal additional structure within the lines, were taken. However, this structure does not show a significant dependence on the orbital phase, as seen from the trailed spectra depicted in Figure 8.

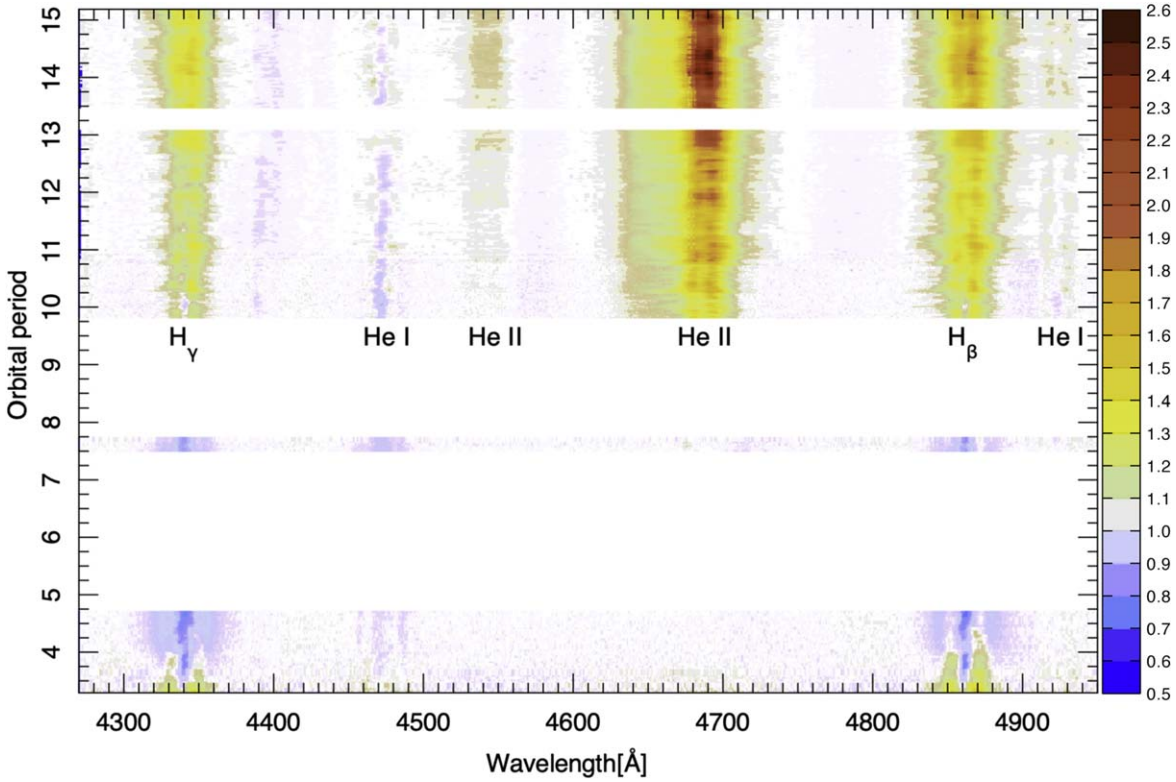

Figure 5. The trailed spectrogram of the object encompasses the rise to the superoutburst. It shows the evolution of lines, a transformation from emission (yellow-red hue) to absorption (grayish-blue hue) and back, a change in the widths and intensity, as well as the emergence of He II lines. The time axis is given in units of orbital periods, starting from the first spectrum taken during the superoutburst.

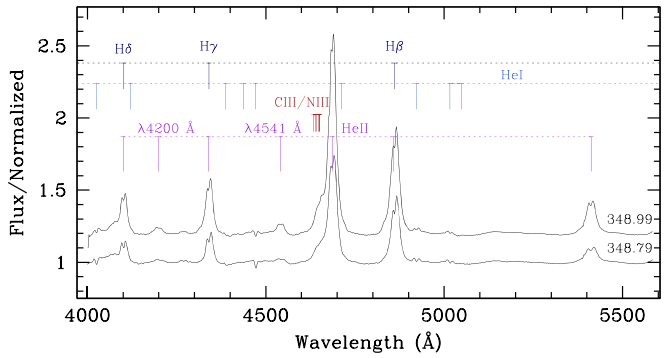

Figure 6. Examples of spectra during the last stages of the rise between labels 5 and 6 (see Table 2) obtained in the 4000–5600 Å range. A strong increase in the strength of the He II λ4686 emission line is accompanied by the emergence of He II λ4200,4540. Spectral lines are labeled above two averaged and time-stamped spectra corresponding to the beginning and end of the observing run.

The lines observed in high resolution are shown in Figure 9. An absorption feature is distinctly detected in the center of the He I lines and, less marked, in He II. The Hα line was not observed in the lower-resolution spectra but was covered by the echelle data. Practically no central absorption is visible in Hα, which also argues against an origin from within the accretion disk. A compact spot can be seen in the Doppler map of the Hα line (upper-right panel of Figure 8); it is larger for Hβ and becomes a ring-like feature in the case of He II (upper-right and bottom-left panels, respectively). The latter forms practically a perfect circle positioned right at the center of mass of the system. Such a pattern is formed in the tomograms of all major lines, once the object reaches the peak of the outburst, except for He I. Trailed spectra and tomograms obtained with higher resolution seem to confirm that there are no pronounced radial velocity variations in the lines that could have been lost due to the lower spectral resolution. However, the analysis, described in Section 5 shows that there are multiple modulations invisible to the eye.

4.6. The Decline

We followed the spectral evolution of the V455 And superoutburst for about 60 days after the peak. The decline light curves resemble a skiing slope, a rapid descent for about 10 days followed by a gradual flattening before an abrupt plunge of almost two magnitudes (see Figure 1). After that sudden drop, the gradual decline continues. In some WZ Sge–type superoutbursts, secondary or repetitive rebrightenings are observed[4] (also known as echoes) (Patterson et al. 1998). Without going into details of superoutburst morphology and contested explanations, it is worth noting that the plunge most probably corresponds to the transition of the accretion disk to the cool, quiescent state as a result of the accretion rate dropping below the critical instability level (e.g., Smak 1993).

In Figure 10, we present the spectral evolution of V455 And from the outburst peak to the various stages of decline and a representative spectrum of the object in quiescence, 1 yr after the superoutburst. The spectra are flux-calibrated, and the flux decreases as the object declines from the outburst from the top to the bottom of Figure 10. Each spectrum has been averaged

[4] According to Kato (2015, and references therein), rebrightenings are usually observed soon after the main superoutburst with a long plateau stage. It is classified into five types by the morphology of light curves: type A (long-duration rebrightening), type B (multiple rebrightenings), type C (single rebrightening), type D (no rebrightening), and type E (double plateaus).

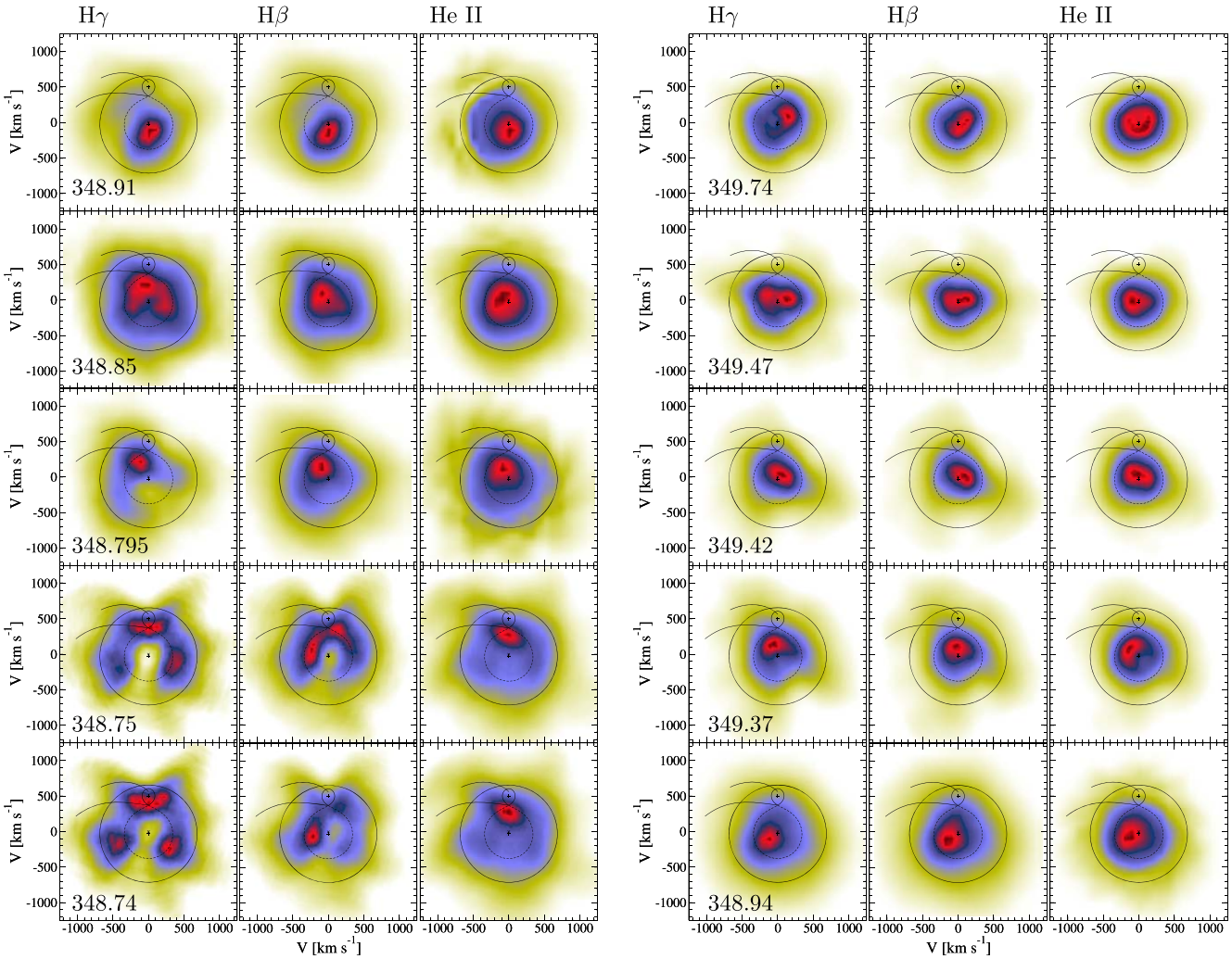

Figure 7. Evolution of Doppler maps of V455 And between labels 5 and 7 (Table 2) (all overlays have the same meaning as in Figure 2). Each tomogram covers one orbital period. The tomograms are placed in chronological order from bottom up, from left to right. HJD of the orbit center is marked in each panel. In the first column from the left are tomograms of the Hγ line, in the middle Hβ, and in the third panel is He II. The trailed spectra of all lines are presented in Figure 5.

for at least one orbital period. The median Julian dates of the observations are marked on the right side. In the middle of the figure, a gap is formed due to the plunge in brightness. The major lines detected in the spectra are marked in that space. As the brightness diminishes, the intensity of the emission lines decreases, and a strong absorption trough develops in the centers of the lines. This transition takes place before the knee in the light curve. As a result, the dense spot, concentrated in the center of mass during the peak, expands, forming a ring in the tomograms as shown in Figure 11. In this figure, we show the Doppler tomograms of four major lines during three nights on the decline plateau. By the HJD 362, the ring corresponding to a disk is already reappearing. We highlight three critical features: (1) The dense spot with a zero velocity, formed at the maximum of the outburst, starts to expand—in a reverse fashion—into a ring. The ring expands and after 12 days the velocities of the inner and outer edges reach those detected in the quiescence. In other words, there is little doubt we are already seeing the accretion disk producing emission lines. (2) The disk emits in the Balmer lines and He II; the latter is not seen in quiescence or after the knee in the light curve. (3) There is a noticeable void in the first quadrant ($V_x = -300$ km s^{-1}, $V_y = -600$ km s^{-1}), while the upper arc (positive V_y) is brighter than the rest of the disk. Indeed, some concentrations are related to the irradiated secondary and hot spot. Nevertheless, the upper-right part of the disk not associated with the spot or secondary is brighter, too. These could be related to the spirals, though.

Detection of He II emission from the entire disk is quite unusual. The He II line source in nonmagnetic CVs is normally limited to the hot spot, irradiated secondary, or associated with the WD or boundary layer (Williams & Ferguson 1982; Williams 1989; Martinez-Pais et al. 1996). Figures 7–11 show the evolution of the He II line. In particular, during the days of HJD 361–362 the Doppler tomograms (see Figure 11), show a complex picture: a hot spot and maybe irradiation of the secondary and the entire ring corresponding to the disk. It is transient, being detected during a short interval during the decline; hence, it is difficult to interpret. It is probable, though, that the emission is formed in a hot, ionized plasma above the disk, rather than in the disk itself, which is still in the upper steady-state stability branch of the temperature–surface-density curve describing accretion disks in CVs. On the other hand, the hot spot and other visible structures are probably within the disk.

After the abrupt plunge, the shape of the spectrum changes significantly, resembling a quiescent spectrum, although brighter. We assume that after the knee, much of the fading

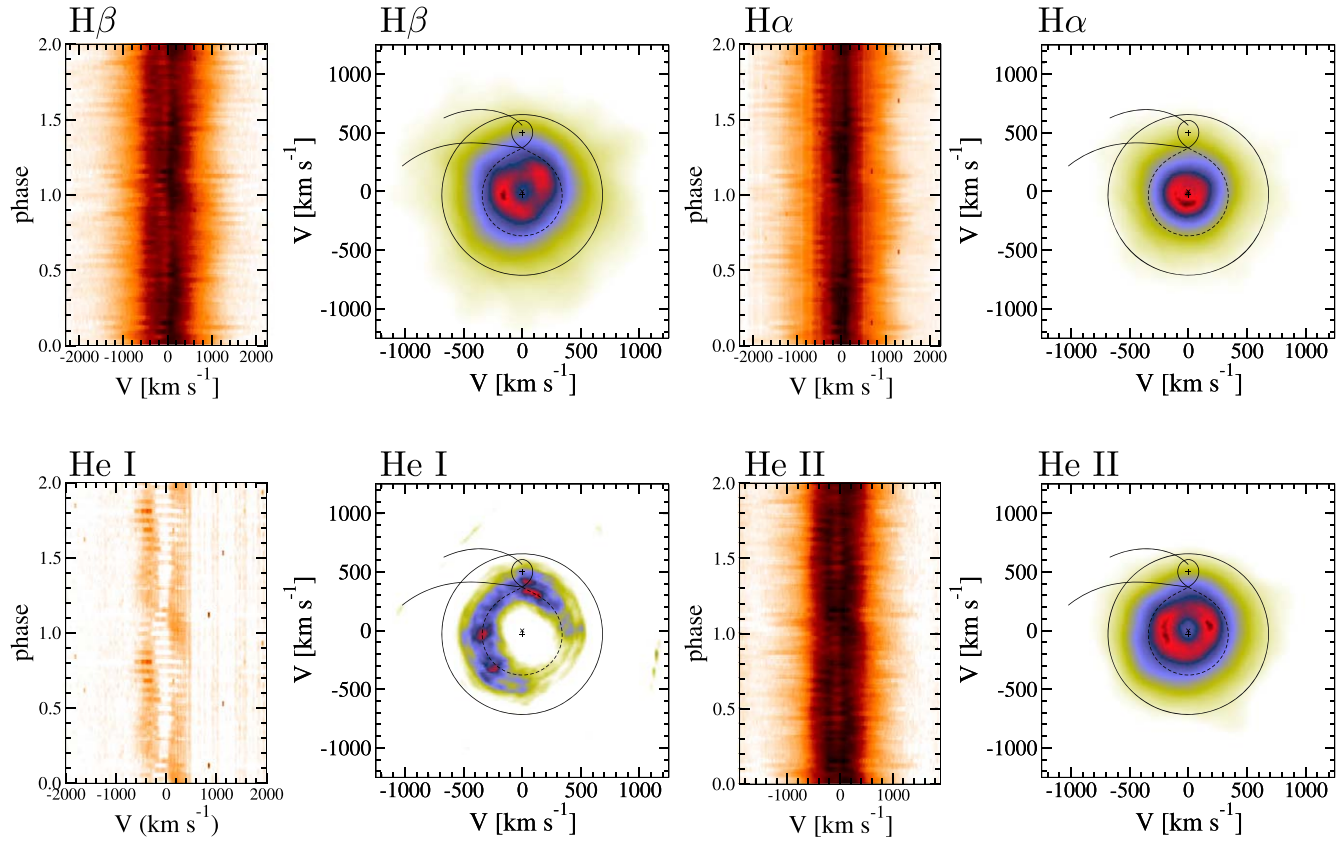

Figure 8. Doppler maps at the peak of the outburst (all overlays have the same meaning as in Figure 2). The trailed spectra and Doppler maps of Hα, Hβ (upper panel), and He I and He II (bottom panel) are presented left to right. The trailed spectra and tomograms are constructed from the high-resolution spectra obtained around HJD 349.8.

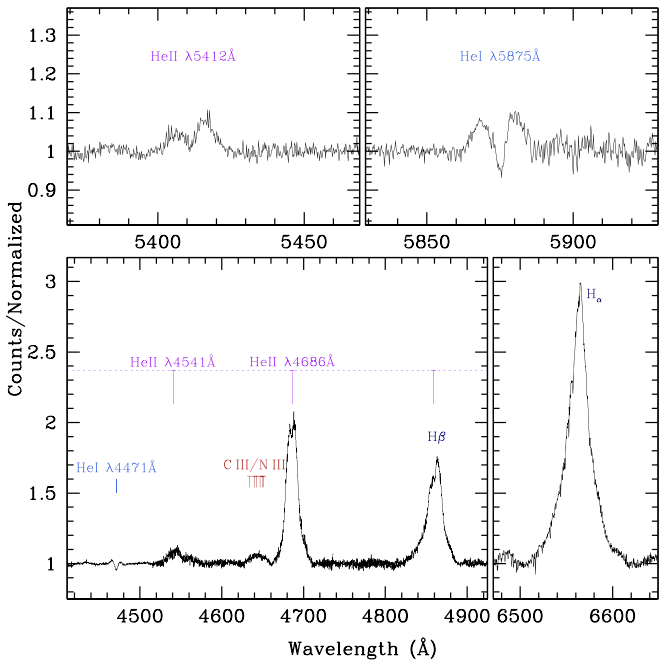

Figure 9. Average of the high-resolution spectroscopy obtained at the maximum of the outburst. Spectral lines are marked. Note the difference in scales.

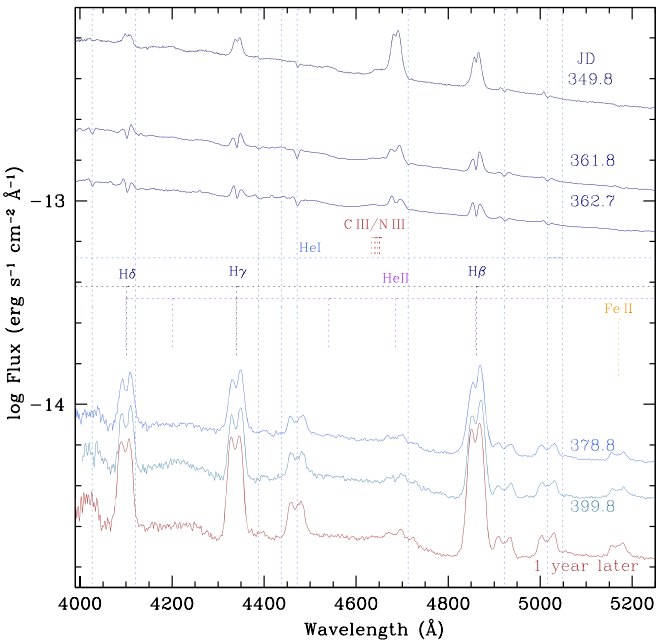

Figure 10. The transition from wind spectrum to quiescence. The He II line is mostly gone; the Balmer lines restore their strength relative to the still elevated continuum. Around HJD 379, the profiles also contain a narrow peak formed by the heated secondary. One year later (the bottom spectrum), the continuum has diminished more as contribution from the secondary vanish, too.

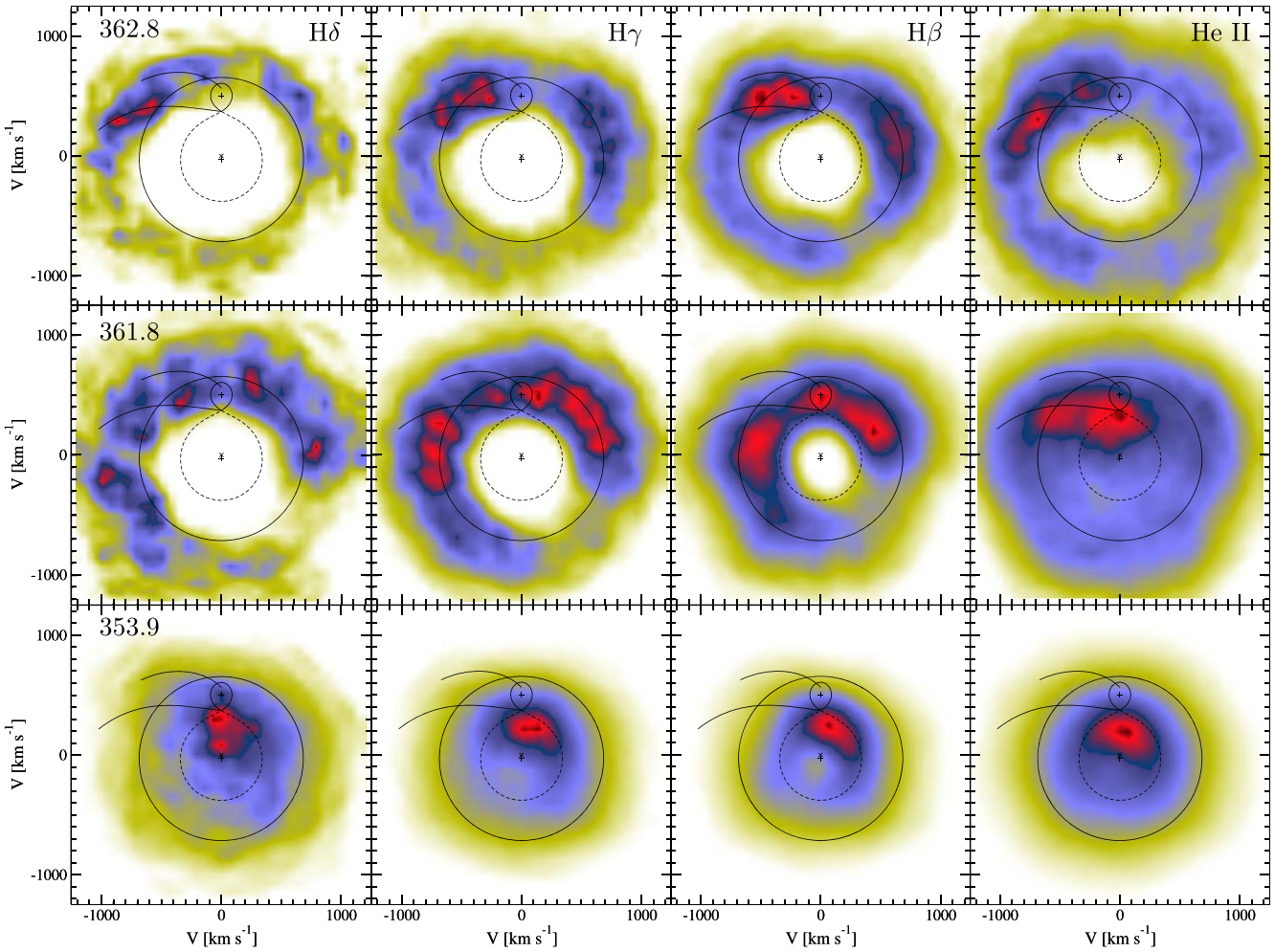

Figure 11. Evolution of Doppler maps of V455 And in the early stages of decline (all overlays have the same meaning as in Figure 2). Each tomogram covers several orbital periods during the entire night. Three nights corresponding to HJD 353, 361, and 362 from bottom to top are presented. In the first column from the left tomograms of the Hδ line are presented, then Hγ, Hβ, and in the last panel is He II.

is related to the (quasi-exponential) cooling of the white dwarf (Szkody et al. 2013). We obtained one full orbital period of a phase-resolved set of spectra around HJD 378.8 about 30 days after the maximum and two weeks after the sharp brightness drop. The general aspect of the spectrum is shown in Figure 10. Most notably, the He II diminishes together with the UV excess. All other lines tower above the continuum and assume a double-peaked shape proper to the accretion disk spectrum of a high-inclination system. Multiple He I and Fe II λ5170 lines also have similar shapes. The latter ion is not typical for CVs but is detected persistently in the quiescent spectra of V455 And. Trailed spectra of Hβ and Hγ lines with their corresponding Doppler tomograms for this date are presented in Figure 12. Also restored is an S wave inside the emission lines. There are two crucial differences between these and the pre-outburst (quiescent) spectra and tomograms presented in Figure 2. First, the phase of a prominent S wave is different from the one observed in the quiescence stage. Evidently, this S wave is not produced by the hot spot but comes from the heated face of the donor star. Unlike the Doppler tomograms from the previous observations, here it is just one concentrated spot coinciding well with the heated face of the secondary star.

5. Long Spectroscopic Period during Superoutburst

An LSP is persistently observed during quiescence (G. Tovmassian et al. 2022, in preparation). It is visible by the eye in the quiescent trailed spectra. It can also be quantified by measuring the radial velocity of the wings of the emission lines using the double-Gaussian method (Tovmassian et al. 2007). During superoutburst, the LSP visually disappears. Emission lines have extended wings to up to 2000 km s^{-1}. We explored the line profiles of high-resolution echelle spectra taken on HJD 349 by fitting them with a Voigt profile.[5] The Voigt results from the convolution of two broadening mechanisms, one of which alone would produce a Gaussian profile (usually, as a result of the Doppler broadening) and the other (of not defined origin) would produce a Lorentzian profile. In this way, we achieve a better fit to the complex lines since both central parts and the wings are considered. We analyzed the fluctuations of line-center velocities for the presence of periodic signals. We used the Lomb-Scargle (Lomb 1976; Scargle 1989) method. Figure 13 presents the power spectrum derived from these measurements of Hβ and Hα lines (the dark blue and red

[5] Spectra of HJD 349 were obtained with 240 s exposure times for 6.55 hr (see Table 1).

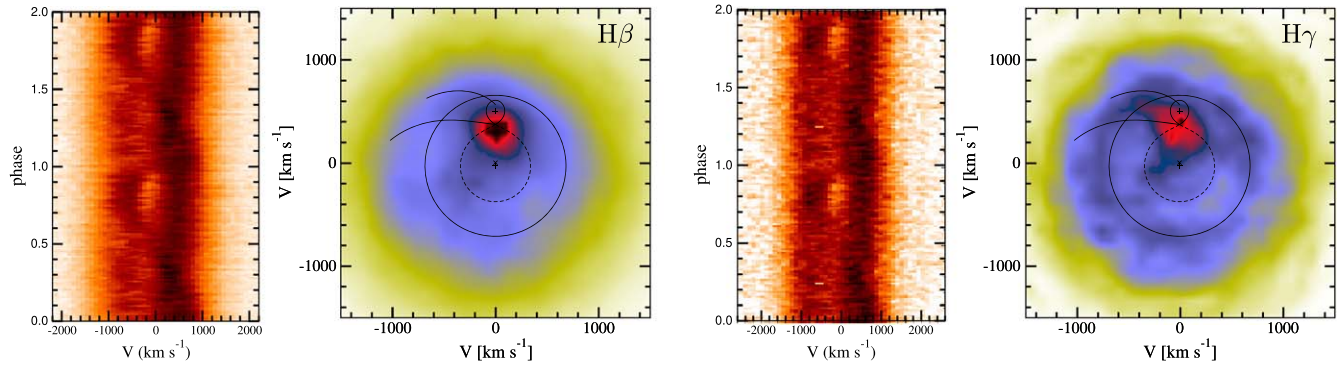

Figure 12. Doppler maps of V455 And during the decline from the outburst (all overlays have the same meaning as in Figure 2). From left to right, the trailed spectra and Doppler maps of Hβ and Hγ are presented. The trailed spectra and tomograms are constructed from the spectra obtained around HJD 2454378.85.

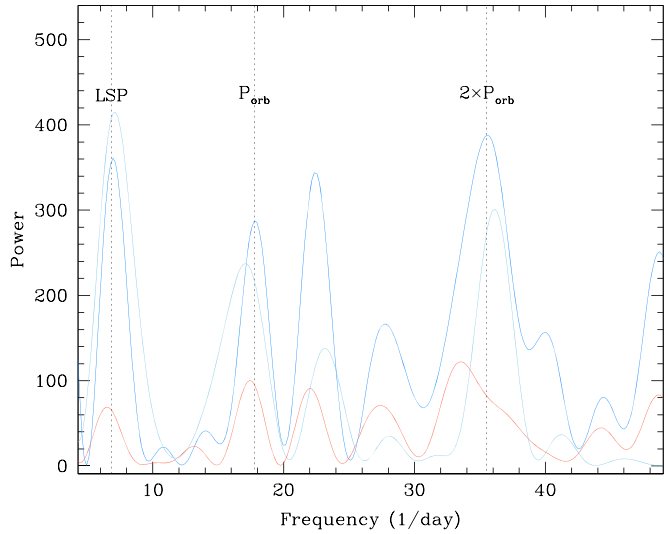

Figure 13. Power spectra of RV measurements of Hβ (blue lines) and Hα (red). The dark blue and red curves correspond to high-resolution observations of the outburst's maximum (HJD 349). The light blue curve is the power spectrum of Hβ from HJD 378 medium-resolution spectra. The latter was scaled (0.25×) for the sake of presentation. Vertical dashed lines mark the major known frequencies.

curves correspondingly). There are a variety of comparable strong peaks. Clearly visible are the orbital period ($P_{\rm orb}$) and its harmonic ($2 \times P_{\rm orb}$). The strong appearance of the latter in the power spectrum of RVs is somewhat confusing because, unlike the light curve, the RV should primarily be modulated on the orbital period. Any signal at $2 \times P_{\rm orb}$ arising from a slight deviation from a sine curve should appear weaker in the power spectrum. In fact, the power spectrum of the FWHM of the Gaussian components (not shown) contains a dominating peak at the orbital period.

The strong peak seen in the power spectrum of Hβ is close to the mean value of the LSP determined from quiescent observations. Intrigued by this finding, we also measured the RVs of the Hβ line in the spectra from HJD 378, i.e., in the advanced decline stage. We used a single Gaussian in this analysis as the line wings are not as extended as at the outburst peak, and as the spectral resolution of these observations is lower. The resulting periodogram is similar to that obtained during the outburst peak (see the light blue curve in Figure 13), including the detection of the LSP, which is, in fact, the strongest signal at that stage of the outburst. The peaks at 6.96 and 7.11 day^{-1} on HJD 349 and HJD 378 correspondingly, are within the range of LSP frequencies detected during quiescence.

Regardless of the exact physical mechanism underlying the LSP, it has to be formed in the central parts of the disk. Tovmassian et al. (2007) proposed that it reflects the beam from the precessing magnetic WD by the inner parts of the truncated disk, and Gänsicke (2007) suggested magnetic curtains of the precessing inner disk as a source of this unusual phenomenon. During the superoutburst, the conditions in the disk change drastically. The optical depth, viscosity, temperature, and density experienced sudden changes. Nevertheless, the LSP persists, as demonstrated by the detection in the RV periodograms. We are still oblivious as to the actual physical mechanism behind the LSP, but any suggested explanation will have to work both in quiescence and during the peak of the outburst. An additional clue is that the LSP was not present in the power spectrum of the He II RVs.

6. The Interpretation

The most unusual observation in the course of the superoutburst of V455 And was the emergence of strong emission lines with narrow and almost single peaks during the rise of the outburst, starting before the peak and lasting until about 10 days after the maximum.

The spectral behavior of DNe during outbursts is well understood in general terms. In quiescence, the disk is mostly optically thin in the continuum, and DNe are characterized by intense Balmer emission lines accompanied by weaker neutral and sometimes ionized helium lines. Usually, no other strong lines are present. The width of emission lines, which arise from the entire disk, depends primarily on the inclination angle, but their shape is double-peaked unless the system is seen almost face-on. The double-peaked lines show little RV variability because the amplitude of the central object is small, and there is a significant gradient of velocities in the disk. In order to measure the motion of the central object (WD), the RV of the extremes of the wings, formed near the WD, are often measured. In addition to the double-peaked line a narrow emission component is often detected (formed in the hot spot where the accretion stream impacts the disk) showing a sinusoidal pattern swinging back and forth between the double peaks. During an outburst, the disk quickly becomes hot and dense; its spectrum then resembles those of novalikes: broad absorption lines from the optically thick disk with weak central emission peaks. Typically, absorption is stronger in higher members of the Balmer series, while emission prevails toward

the lower lines of the series, particularly in Hα (e.g., Hessman et al. 1984, Figure 5). The emission peaks in novalikes are formed in a variety of spots, depending on the geometry and physical parameters of the particular system. Although CVs are notorious for peculiarities, such behavior during outbursts is universally observed in DNe, including during WZ Sge–type superoutbursts. Until now, all other WZ Sge stars observed in the outburst (Nogami & Iijima 2004; Nogami et al. 2009) show absorption lines during the maximum and the plateau phases.

In the case of the superoutburst of V455 And, the behavior was entirely different. V455 And suddenly deviated from the usual behavior and converted from an absorption-dominated spectrum into one with intense emission lines. It includes the emergence of high-ionization-level He II λ4686 and λ5412 not observed in this object in quiescence or the early stages of the superoutburst. The profiles of the lines also changed, with a wide basis but sharp, nearly single-peaked cores (Figure 9). The only species that did not undergo such transformation were numerous neutral helium lines.

6.1. Accretion Disk Wind

The observed emergence of strong emission lines, including the He II lines, are consistent with the concept of evaporation from the surface of the accretion disk and the formation of an accretion disk wind. This idea was first proposed by Tovmassian et al. (2011), suggesting that the observed profiles of spectral lines during the superoutburst of V455 And are compatible with the emergence of an accretion disk wind. Mass outflows often accompany accretion disks in binaries. Accretion disk winds in low-mass X-ray binaries are universally recognized and can be of the order of, or larger than, the mass accreted into the system during the outflows (Ponti et al. 2012). Winds also occur in active galactic nuclei (AGNs) and young stellar objects (YSOs). In the case of CVs, a key evidence for outflows comes from P Cygni profiles of strong UV lines. The first evidence was reported by Heap et al. (1978), and since then, many others have studied it (e.g., Cordova & Mason 1982). Evidence of winds is not limited to the UV lines; on rare occasions, it can be detected in the optical range (Kafka & Honeycutt 2004; Honeycutt et al. 2013).

Single-peaked lines in optical spectra of high-inclination novalikes have been considered as evidence of winds. The modeling efforts were mostly concentrated on explaining this phenomenon in certain systems, most notably RW Tri (Matthews et al. 2015). However, Subebekova et al. (2020) showed by means of high-resolution spectroscopy that single-peaked lines in fact comprise two components. In three additional novalikes with vastly different inclination angles (Hernandez et al. 2017; Hernández et al. 2021), a similar structure of emission lines was revealed.

On the other hand, Inight et al. (2022) recently detected a wind in the optical spectra of the novalike variable ASAS J071404+7004.3 in the form of a P Cygni profile in He I λ5876. All emission lines in that system are single peaked. and the authors argued that they arise within the wind. P Cygni profiles are, of course, strong evidence for the presence of wind. However, the P Cygni profile is reported to be very transitional in this object, while emission peaks are of a more consistent nature. The former can be the result of a clumpy flow of the wind (Proga et al. 2002). It appears that we do not have a good idea in which cases the optical spectra, or what fraction of the emission, correspond to the wind.

A variety of theoretical calculations (Murray & Chiang 1997; Ribeiro & Diaz 2008; Flohic et al. 2012; Matthews et al. 2015) demonstrate that the lines arising from wind have a specific shape depending on the inclination angle and the optical depth in the corresponding line. Although all the authors mentioned above agree on the shape of the lines, they differ in the details regarding the opacity, the density of the wind, etc. Using their calculated line profiles, Ribeiro & Diaz (2008) have created artificial Doppler maps to demonstrate what the tomogram of a disk-wind will look like. From these studies, they find that the higher the opacity of the lines, the smaller the separation of peaks.

In this regard, we draw attention to the rapid contraction of the ring-like structure in the Doppler maps during the rise to the superoutburst depicted in Figure 7. This contraction is a development that cannot be happening inside the disk. As the wind commensurate with the density of the ionized matter increases, opacity in the line increases, too. The outflow probably reaches considerable heights. It all translates into a decreasing separation of peaks of emission lines, eventually getting the form of a bell with an almost single peak. Such a process will lead to the shrinkage of the ring-like structure in Doppler maps. Eventually, at the peak of the outburst, the ring converts to a sharp spot of zero velocity in the Hα tomogram, shown in Figure 8. Hence, the evolution of the Doppler tomograms reflects the transformation of the line profiles in accordance with the wind density increase at the beginning of the outburst and dissipation past maximum. A careful examination of Figure 7 shows that there are also differences in the final pattern of the Doppler maps for different lines (see also Figures 11 and 12, for example). These differences are expected if we assume that the opacity varies from line to line and, hence, produces different peak separation of lines.

Matthews et al. (2015) in disk-wind models obtain a much stronger He II line than is observed in the novalike systems. It looks like, in this case, there is no such discrepancy. Modeling quantitatively the accretion disk wind is not an easy task and the attempts are not numerous. In particular, spectra of V455 And during the superoutburst in terms of an accretion disk wind would be a really difficult problem given the variable nature of the disk luminosity and nonstationary state of the wind. It is beyond the scope of this paper.

The evolution of the line profiles, and hence of the Doppler tomograms obtained during the decline from the outburst, confirms the assumption that the changing emission-line profiles reflect the change in their optical depths. The series of tomograms presented in Figure 11 of the major four lines in the observed spectral range shows a reversal of the evolution detected during the rise. Here, the sharp single-peaked lines split into two peaks with increasing distance between them. This is reflected in the Doppler maps as a rapid widening ring until it reaches the velocities corresponding to the accretion disk. We may assume that the outflow rate falls, leading to the decrease of the outflow density, and hence, the decrease of the optical depth in the lines. By HJD 362.8, 13 days after the peak of the superoutburst, the ring is confined to the border of the accretion disk, marked as a solid circle in all tomograms. However, at this stage, the He II line is still prominent, hinting that the emission lines are still formed above the main body of the accretion disk and partially in the hot spot.

Strong He II emission and the evolution from absorption to emission of Hα before the outburst maximum have also been

observed during the superoutburst of WZ Sge (Nogami & Iijima 2004). They report a smaller separation of peaks of emission lines than during the quiescence. But the rest of the Balmer lines remained mostly in absorption. In the course of the superoutburst of GW Lib, the spectrum shows single-peaked emission lines of Hα, He II, and C III/N III superposed on absorption lines of Balmer components and He I. Several other spectroscopic snapshots of outbursts of WZ Sge objects report predominantly absorption lines in spectra during the maximum brightness (e.g., Onori et al. 2016; Gromadzki et al. 2017; Isogai et al. 2019). These authors argue that the emission lines are formed in the chromosphere of the accretion disk by irradiation.

V455 And, of course, is not the only system where there is an outflow from the surface of the disk amounting to the wind; but this detection is a rare occasion in which we were able to see the rise of the wind hours after the start of the superoutburst and its demise 2 weeks later.

6.2. Irradiated Secondary Star

Two weeks later into the decline (three weeks after maximum), when we returned to obtain more spectra, we found no He II line after the gap in the data already mentioned in Section 4.6 (see Figure 10 at HJD 378.8). The spectra mostly resembled those in quiescence, but with one notable exception: There was an additional component in the emission-line profiles of Hβ and Hγ, which coincided with the expected position of the secondary in the Doppler maps. This is shown in Figure 12 (already discussed in Section 4.6) of the tomograms constructed from spectra taken on day HJD 378.8 and which show a concentrated spot at $V_x = 10 \pm 32$, $V_y = 303 \pm 32$ km s^{-1}. Within errors, this value matches the L_1 velocity derived from the dynamical constraints by G. Tovmassian et al. (2022, in preparation), and hence corresponds to the heated side of the secondary star according to the orbital phase among other parameters. The irradiated secondary with similar velocities was also spotted during the decline from the 2001 superoutburst of WZ Sge (Steeghs et al. 2001).

7. Conclusions

We performed an intense spectroscopic campaign of the 2007 superoutburst of V455 And, a bona fide WZ Sge–type dwarf nova. We were able to densely cover the rise to the superoutburst, which is unprecedented thus far in the study of dwarf nova outbursts, particularly superoutbursts. Our observations show that several hours into the start of the superoutburst, halfway to the peak of the superoutburst, the spectral behavior suddenly experienced a dramatic change. The emergence of all Balmer and ionized helium lines in emission, their intensities, and the evolution of their profiles during the rise and throughout the early decline allow us to conclude that we are witnessing the emergence of a powerful accretion disk wind. We argue that the emission lines at this stage do not form in the accretion disk but above it. The fast and continuous reduction of the distance between the line peaks during the rise, and the increase during the decline, is interpreted as growth of the line opacity. The wind is launched as the disk turns dense and hot, and fades as the disk cools down and the surface density drops.

P Cygni profiles in novalikes have been detected in isolated observations. The absence of P Cygni profiles in the optical spectrum could be explained by the stratification of ionization and the line formation region being at a large distance from the orbital plane. Nondetection of P Cygni profiles during these observations does not contradict the hypothesis that we observed an episode of intense accretion disk wind during the superoutburst of V455 And.

Nevertheless, Hβ emission at the peak of the superoutburst, and days later, shows the presence of modulation with several previously known periods, which is inconsistent with the idea that the line is entirely formed by the wind. The detection of a set of periods is incomprehensible, and it is impossible to estimate what fraction of the line is solely produced by the wind.

While this paper was being prepared, Tampo et al. (2022) published an observational study on V455 And, and, although they only cover the superoutburst from the maximum and decline, they reached similar conclusions with respect to the wind outflow. Here, we covered the complete rise to the outburst, which is absent in their study. Hence we have described all observational features during the superoutburst in great detail.

We also detected the heated secondary star during the decline from the superoutburst and confirmed the correctness of system parameters drawn in G. Tovmassian et al. (2022, in preparation). Several issues have to wait for further studies, including the mysterious LSP.

Based upon observations carried out at the Observatorio Astronómico Nacional on the Sierra San Pedro Mártir (OAN SPM), Baja California, México. G.T. is grateful for continuous support from CONACyT grants 34521-E, 151858, and 166376, as well as PAPIIT grants IN107712, 108316, and 110619. J.E. is indebted to DGAPA (Universidad Nacional Autónoma de México) for continuous support with PAPIIT grants IN111713, IN122409, IN114917, and IN103120. S.Z. acknowledges PAPIIT grants IN102120. This research has been funded in part by the Science Committee of the Ministry of Education and Science of the Republic of Kazakhstan (grant No. AP08856419). B.T.G. was supported by grant ST/T000406/1 from the Science and Technology Facilities Council (STFC). This project has received funding from the European Research Council (ERC) under the European Union's Horizon 2020 research and innovation program (grant agreement No. 101020057). We would like to thank the anonymous reviewer whose comments helped to greatly improve this paper.

Facilities: ING:Herschel, OANSPM:0.8 m, OANSPM:2.1 m, AAVSO.

ORCID iDs

Gagik Tovmassian https://orcid.org/0000-0002-2953-7528
Boris T. Gänsicke https://orcid.org/0000-0002-2761-3005
Juan Echevarria https://orcid.org/0000-0001-5960-3023
Sergey Zharikov https://orcid.org/0000-0003-2526-2683

References

Araujo-Betancor, S., Gänsicke, B. T., Hagen, H.-J., et al. 2005, A&A, 430, 629
Bailey, J. 1979, MNRAS, 189, 41P
Bertin, E., & Arnouts, S. 1996, A&AS, 117, 393
Bloemen, S., Steeghs, D., De Smedt, K., et al. 2013, MNRAS, 429, 3433
Cheng, F. H., & Lin, D. N. C. 1992, ApJ, 389, 714
Cordova, F. A., & Mason, K. O. 1982, ApJ, 260, 716
Echevarría, J., Costero, R., Tovmassian, G., et al. 2002, in AIP Conf. Ser. 637, Classical Nova Explosions, ed. M. Hernanz & J. José (Melville, NY: AIP), 77

Echevarría, J., Diego, F., Martínez, A., et al. 1989, RMxAA, 17, 15
Flohic, H. M. L. G., Eracleous, M., & Bogdanović, T. 2012, ApJ, 753, 133
Gaia Collaboration, Brown, A. G. A., Vallenari, A., et al. 2018, A&A, 616, A1
Gänsicke, B. T. 2007, in AIP Conf. Ser. 372, 15th European Workshop on White Dwarfs, ed. R. Napiwotzki & M. R. Burleigh (Melville, NY: AIP), 597
Gromadzki, M., Wyrzykowski, L., Mroz, P., et al. 2017, ATel, 10389, 1
Hameury, J.-M. 2019, AdSpR, 66, 1004
Hameury, J. M., & Lasota, J. P. 2017, A&A, 602, A102
Heap, S. R., Boggess, A., Holm, A., et al. 1978, Natur, 275, 385
Hellier, C. 2002, AIP Conf. Ser. 261, The Physics of Cataclysmic Variables and Related Objects, ed. B. T. Gänsicke, K. Beuermann, & K. Reinsch, 92, arXiv:astro-ph/0201475
Hernández, M. S., Tovmassian, G., Zharikov, S., et al. 2021, MNRAS, 503, 1431
Hernandez, M. S., Zharikov, S., Neustroev, V., & Tovmassian, G. 2017, MNRAS, 470, 1960
Hessman, F. V., Robinson, E. L., Nather, R. E., & Zhang, E. H. 1984, ApJ, 286, 747
Honeycutt, R. K., Kafka, S., & Robertson, J. W. 2013, AJ, 145, 45
Inight, K., Gänsicke, B. T., Blondel, D., et al. 2022, MNRAS, 510, 3605
Isogai, K., Kawabata, M., Burgaz, U., Maeda, K., & Maehara, H. 2019, ATel, 13161, 1
Isogai, M., Arai, A., Yonehara, A., et al. 2015, PASJ, 67, 7
Kafka, S. 2021, Observations from the AAVSO International Database, https://www.aavso.org
Kafka, S., & Honeycutt, R. K. 2004, AJ, 128, 2420
Kato, T. 2015, PASJ, 67, 108
Kimura, M., Kato, T., Imada, A., et al. 2016, PASJ, 68, L2
Kuulkers, E., Henden, A. A., Honeycutt, R. K., et al. 2011, A&A, 528, A152
Kuulkers, E., Knigge, C., Steeghs, D., Wheatley, P. J., & Long, K. S. 2002, in AIP Conf. Ser. 261, The Physics of Cataclysmic Variables and Related Objects, ed. B. T. Gänsicke, K. Beuermann, & K. Reinsch, 443
Lin, D. N. C., & Papaloizou, J. 1979, MNRAS, 186, 799
Liu, W., Li, Z. Y., & Hu, J. Y. 1997, Ap&SS, 257, 183
Lomb, N. R. 1976, Ap&SS, 39, 447
Maehara, H., Imada, A., Kubota, K., et al. 2009, in AIP Conf. Ser. 404, The Eighth Pacific Rim Conf. Stellar Astrophysics: A Tribute to Kam-Ching Leung, ed. B. Soonthornthum et al. (Melville, NY: AIP), 57
Marsh, T. R., & Horne, K. 1988, MNRAS, 235, 269
Martinez-Pais, I. G., Giovannelli, F., Rossi, C., & Gaudenzi, S. 1996, A&A, 308, 833
Matsui, R., Uemura, M., Arai, A., et al. 2009, PASJ, 61, 1081
Matthews, J. H., Knigge, C., Long, K. S., Sim, S. A., & Higginbottom, N. 2015, MNRAS, 450, 3331
Meyer, F., & Meyer-Hofmeister, E. 1981, A&A, 104, L10
Meyer, F., & Meyer-Hofmeister, E. 2015, PASJ, 67, 52
Mineshige, S., & Osaki, Y. 1983, PASJ, 35, 377
Morales-Rueda, L., & Marsh, T. R. 2002, MNRAS, 332, 814
Murray, N., & Chiang, J. 1997, ApJ, 474, 91
Neustroev, V. V., & Zharikov, S. V. 2020, A&A, 642, A100
Nogami, D., Hiroi, K., Suzuki, Y., et al. 2009, AIP Conf. Ser. 404, The Eighth Pacific Rim Conference on Stellar Astrophysics: A Tribute to Kam-Ching Leung, ed. B. Soonthornthum et al., 52
Nogami, D., & Iijima, T. 2004, PASJ, 56, S163
Onori, F., Lena, D., Kostrzewa-Rutkowska, Z., et al. 2016, ATel, 9226, 1
Osaki, Y. 1995, PASJ, 47, 47
Paczynski, B. 1977, ApJ, 216, 822
Patterson, J., Kemp, J., Skillman, D., et al. 1998, PASP, 110, 1290
Ponti, G., Fender, R. P., Begelman, M. C., et al. 2012, MNRAS, 422, L11
Proga, D., Kallman, T. R., Drew, J. E., & Hartley, L. E. 2002, ApJ, 572, 382
Ribeiro, F. M. A., & Diaz, M. P. 2008, PASJ, 60, 327
Scargle, J. D. 1989, ApJ, 343, 874
Smak, J. 1982, AcA, 32, 199
Smak, J. 1993, AcA, 43, 101
Spruit, H. C. 1998, arXiv:astro-ph/9806141
Steeghs, D. 2004, RMxAA, 20, 178
Steeghs, D., Marsh, T., Knigge, C., et al. 2001, ApJL, 562, L145
Subebekova, G., Zharikov, S., Tovmassian, G., et al. 2020, MNRAS, 497, 1475
Szkody, P., Mukadam, A. S., Gänsicke, B. T., et al. 2013, ApJ, 775, 66
Szkody, P., Silber, A., Sion, E., et al. 1996, AJ, 111, 2379
Tampo, Y., Nogami, D., Kato, T., et al. 2022, PASJ, 74, 460
Tovmassian, G., Gänsicke, B., Zharikov, S., et al. 2011, in Jets at all Scales, IAU Symp. 275 (Cambridge: Cambridge Univ. Press), 311
Tovmassian, G. H., Zharikov, S. V., & Neustroev, V. V. 2007, ApJ, 655, 466
van Spaandonk, L., Steeghs, D., Marsh, T. R., & Torres, M. A. P. 2010, MNRAS, 401, 1857
Warner, B. 1995, Cataclysmic Variable Stars, Vol. 28 (Cambridge: Cambridge Univ. Press)
Williams, R. E. 1989, AJ, 97, 1752
Williams, R. E., & Ferguson, D. H. 1982, ApJ, 257, 672